CHAPTER 1

The theory of Turing pattern formation

Teemu Leppänen

Helsinki University of Technology, Laboratory of Computational Engineering
P.O.Box 9203, FIN-02015 HUT, FINLAND E-mail: teemu.leppanen@hut.fi

In this article the theory behind Turing instability in reaction-diffusion systems is reviewed. The use of linear analysis and nonlinear bifurcation analysis with center manifold reduction for studying the behavior of Turing systems is presented somewhat meticulously at an introductory level. The symmetries that are considered here in the context of a generic Turing model are the two-dimensional hexagonal lattice and three-dimensional SC- and BCC-lattices.

1. Introduction

The self-organization of dissipative structures is a phenomenon typical to non-equilibrium systems. These structures exist far from equilibrium and differ from typical equilibrium structures (eg. crystals) in that they are kept in the steady-state by competing ongoing dynamic processes, which feed energy into the system. The structures persist by dissipating the input energy (and thus generating entropy), which makes the process irreversible. Dissipative structures are typically macroscopic and the characteristic length scale of the structure is independent of the size of the individual constituents (eg. molecules) of the system. The systems representing self-organized dissipative structures vary from growing bacterial colonies to fluids with convective instabilities (eg. Rayleigh-Bénard convection).[1,2]

The formal theory of self-organization is based on non-equilibrium thermodynamics[3] and was pioneered by chemist Ilya Prigogine. Most of the research was made in Brussels from the 1940s to 1960s by Prigogine and coworkers. They extended the treatment of non-equilibrium thermodynamic systems to nonlinear regime far from equilibrium and applied bifurcation theory to analyze the state selection.[4] Already in 1945 Prigogine had suggested that a system in non-equilibrium tries to minimize the rate of entropy production and chooses the state accordingly.[5] This condition was proved inadequate by Rolf Landauer in 1975, who argued that minimum entropy production is not in general a necessary condition for the steady-state and that one cannot determine the most favorable state of the system based on the behavior in the vicinity of the steady state, but one must consider the global non-equilibrium dynamics.[6] Nevertheless, in 1977 Prigogine was

awarded the Nobel price in chemistry for his contribution to the theory of dissipative structures.

This article does not deal with the so far incomplete theory of non-equilibrium thermodynamics, but with chemical systems, which can exhibit instabilities resulting in either oscillatory or stationary patterns.[7,8] The difficulties of non-equilibrium thermodynamics are also present in the theory of chemical pattern formation. We will specifically concentrate in systems showing so called Turing instability, which arises due to different diffusion rates of reacting chemical substances. Turing instability can be thought as a competition between activation by a slow diffusing chemical (activator) and inhibition by a faster chemical (inhibitor). The idea of diffusion-driven instability was first discussed by Nicolas Rashevsky in 1938[9], but the renown British mathematician and computer scientist Alan Turing has earned most of the fame for giving the first mathematical treatment and analysis of such a model in 1952.[10]

Turing's motivation for studying the chemical system was biological and consequently the seminal paper was titled *The Chemical Basis of Morphogenesis*, where he called the reacting and diffusing chemicals *morphogens*. Turing emphasized that his model is very theoretical and a severe simplification of any real biological system, but he was still confident that his model could explain some of the features related to the spontaneous symmetry-breaking and morphogenesis, i.e., the growth of form in nature. Turing neglected the mechanical and electrical aspects and considered the diffusion and reaction of morphogens in the tissue to be more important.[10] Nowadays, there is some qualitative evidence of the capability of Turing models to imitate biological self-organization[11,12,13], but the conclusive proof that morphogenesis is indeed a Turing-like process is still missing.

The problem of Turing's theory was that the existence of chemical spatial patterns as predicted by his mathematical formulations could not be confirmed experimentally. The existence of Turing patterns in any chemical system could be questioned not to talk about the biological systems. Actually, in the early 1950s a Russian biochemist Boris Belousov observed an oscillation in a chemical reaction, but he could not get his results published in any journal, because he could not explain the results, which were claimed to contradict with the second law of thermodynamics. Prior to Prigogine's work it was held that entropy has to always increase in a process and thus a chemical oscillation was deemed to be impossible with entropy increasing and decreasing by turns. It was not before the late 1960s, when it was noticed that the reaction first observed by Belousov exhibits a pattern formation mechanism with similarities to the mechanism Turing had proposed. However, it is important to notice that the Belousov-Zhabotinsky reaction forms traveling waves, whereas Turing patterns are time-independent.

The first experimental observation of stationary Turing patterns was preceded by theoretical studies[14,15] and the practical development of a new kind of continuously stirred tank reactors.[16] It was not until 1990, when Patrick De Kepper's group

observed a stationary spotty pattern in a chemical system involving the reactions of chlorite ions, iodide ions and malonic acid (CIMA reaction).[17] In particular the required difference in the diffusion rates of the chemical substances delayed the first experimental observation of Turing patterns. In the experiment the condition was achieved by carrying out the experiment in a slab of polymer gel and using a starch indicator, which decreases the diffusion rate of the activator species (iodide ions). In 1991 also stripes were observed in the CIMA reaction and it was shown that experimental Turing patterns can be grown also over large domains.[18]

The observation of Turing patterns initiated a renewed interest in Turing pattern formation. What had previously been only a mathematical prediction of an ingenious mathematician was 40 years later confirmed to be a real chemical phenomenon. This article introduces the reader to the theoretical background and mathematical formalism related to the study of Turing pattern formation. I will introduce the reader to the idea of Turing instability and to the mathematical models that generate Turing patterns in Sec. 2. In Sec. 3 the same topics will be discussed from a more mathematical point of view. In Sec. 4 the methods of the bifurcation theory will be applied to the study of the pattern (2D) or structure (3D) selection in a generic Turing model.

2. Turing instability

The traveling wave patterns generated by the Belousov-Zhabotinsky reaction are not due to Turing instability since the diffusion rates of the chemicals involved in that reaction are usually more or less the same. The difference in the diffusion rates of the chemical substances is a necessary, but not a sufficient condition for the diffusion-driven or Turing instability. Turing's idea that diffusion could make a stable chemical state unstable was innovative since usually diffusion has a stabilizing effect (e.g. a droplet of ink dispersing into water). Intuitively Turing instability can be understood by considering the long-range effects of the chemicals, which are not equal due to difference in the pace of diffusion and thus an instability arises. Some exhilarating common sense explanations of the mechanism of the instability can be found from the literature: Murray has discussed sweating grasshoppers on a dry grass field set alight[11] and Leppänen *et al.* have tried to illustrate the mechanism by using a metaphor of biking missionaries and hungry cannibals on an island.[19]

Turing begun his reasoning by considering the problem of a spherically symmetrical fertilized egg becoming a complex and highly structured organism. His purpose was to propose a mechanism by which the genes could determine the anatomical structure of the developing organism. He assumed that genes (or proteins and enzymes) act only as catalysts for spontaneous chemical reactions, which regulate the production of other catalysts or morphogens. There was not any new physics involved in Turing's theory. He merely suggested that the fundamental physical laws can account for complex physico-chemical processes. If one has a spherically symmetrical egg, it will remain spherically symmetrical forever notwithstanding the

chemical diffusion and reactions. Something must make the stable spherical state unstable and thus cause spontaneous symmetry-breaking. Turing hypotetized that a chemical state, which is stable against perturbations, i.e., returns to the stable state in the absence of diffusion may become unstable against perturbations in the presence of diffusion. The diffusion-driven instability initiated by arbitrary random deviations results in spatial variations in the chemical concentration, i.e., chemical patterns.[10]

No egg in the blastula stage is exactly spherically symmetrical and the random deviations from the spherical symmetry are different in two eggs of the same species. Thus one could argue that those deviations are not of importance since all the organisms of a certain species will have the same anatomical structure irrespective of the initial random deviations. However, Turing emphazised and showed that "it is important that there are some deviations for the system may reach a state of instability in which these irregularities tend to grow".[10] In other words, if there are no random deviations, the egg will stay in the spherical state forever. In biological systems the random deviations arise spontaneously due to natural noise and distortions. A further unique characteristic of the Turing instability is that the resulting chemical pattern (or biological structure) is not dependent on the direction of the random deviations, which are necessary for the pattern to arise. The morphological characteristics of the pattern, e.g. whether it is stripes or spots, are determined by the rates of the chemical reactions and diffusion. That is, the morphology selection is regulated intrinsically and not by external length scales (as in the case of many convective instabilities[2]).

The random initial conditions naturally have an effect on the resulting pattern, but only with respect to the phase of the pattern. The intrinsic parameters determine that the system will evolve to stripes of a fixed width, but the random initial conditions determine the exact positions and the alignment of the stripes (the phase). The relevance of Turing instability is not confined to chemical systems, but also many other physical systems exhibiting dissipative structures can be understood in terms of diffusion-driven instability. Turing instability has been connected to gas discharge systems[20], catalytic surface reactions[21], semiconductor nanostructures[22], nonlinear optics[23], irradiated materials[24] and surface waves on liquids[25]. In this article I will concentrate solely on reaction-diffusion Turing systems.

3. Linear theory

In this section the mathematical formulation of Turing models is introduced, the Turing instability is discussed using mathematical terms and analyzed by employing linear stability analysis. We will witness the strength of linear analysis in predicting the instability and the insufficiency of it in explaining pattern selection. The nonlinear analysis required for explaining pattern selection will be presented in the next section.

Let us denote two space- and time-dependent chemical concentrations by $U(\vec{x},t)$ and $V(\vec{x},t)$, where $\vec{x} \in \Omega \subset \mathbb{R}^n$ denotes the position in an n-dimensional space, $t \in [0,\infty)$ denotes time and Ω is a simply connected bounded domain. Using these notations one can derive a system of reaction-diffusion equations from first principles[11] and they are given as follows

$$\begin{aligned} U_t &= D_U \nabla^2 U + f(U,V) \\ V_t &= D_V \nabla^2 V + g(U,V), \end{aligned} \tag{1}$$

where $U \equiv U(\vec{x},t)$ and $V \equiv V(\vec{x},t)$ are the morphogen concentrations, and D_U and D_V the corresponding diffusion coefficients setting the time scales for diffusion. The diffusion coefficients must be unequal for the Turing instability to occur in two or more dimensions[26]. One should notice that Eq. (1) is actually a system of two diffusion equations, which are coupled via the kinetic terms f and g describing the chemical reactions. This reaction-diffusion scheme is generalizable to any number of chemical species, i.e., equations.

The form of the reaction kinetics f and g in Eq. (1) determines the behavior of the system. These terms can be derived from the chemical formulae describing the reaction by using the law of mass action[11] or devised based phenomenological considerations. There are numerous possibilities for the exact form of the reaction kinetics including the Gray-Scott model[27,28,29,30], the Gierer-Meinhardt model[31], the Selkov model[32,33], the Schnackenberg model[34,35], the Brysselator model[4,36] and the Lengyel-Epstein model[14,37,38]. These all models consist of two coupled reaction-diffusion equations and exhibit the Turing instability within a certain parameter range. The Lengyel-Epstein model is the only one, which corresponds to a real chemical reaction (the experimentally observed CIMA reaction). The presence of some nonlinear term in f and g is common to all these models. A nonlinearity is required since it bounds the growth of the exponentially growing unstable modes.

The stationary state (U_c, V_c) of a model is defined by the zeros of the reaction kinetics, i.e., $f(U_c,V_c) = g(U_c,V_c) = 0$. Typically the models are devised in such a manner that they have only one stationary state, but some models have more. With certain parameters the stationary state is stable against perturbations in the absence of diffusion, but in the presence of diffusion the state becomes unstable against perturbations. If we initialize the system to the stationary state, it will remain there forever. If we perturb the system around the stationary state in the absence of diffusion, the system will return to its original state, i.e., the state is stable. However, when we perturb the system in the presence of diffusion arbitrarily around the stationary state, the perturbations will grow due to the diffusion-driven instability, i.e., the state is unstable. Mathematical definitions of stability can be found from the literature.[40]

All the analysis in this article will be carried out using a generic Turing model introduced by Barrio *et al.*[39] This model is a phenomenological model, where the reaction kinetics are obtained by Taylor expanding the nonlinear functions around

a stationary solution (U_c, V_c). If terms of the fourth and higher order are neglected, the reaction-diffusion equations can be written as

$$\begin{aligned} u_t &= D\delta\nabla^2 u + \alpha u(1 - r_1 v^2) + v(1 - r_2 u) \\ v_t &= \delta\nabla^2 v + v(\beta + \alpha r_1 uv) + u(\gamma + r_2 v), \end{aligned} \tag{2}$$

where the concentrations have been normalized so that $u = U - U_c$ and $v = V - V_c$, which makes $(u_c, v_c) = (0, 0)$ a stationary state. The parameters r_1, r_2, α, β and γ have numerical values and they define the reaction kinetics. The diffusion coefficients are written in terms of a scaling factor δ and the ratio D. We must always have $D \neq 1$ for the instability.

To reduce the number of parameters and simplify the analysis we carry out non-dimensionalization[11] of the Eq. (2) by rescaling the parameters, concentrations and the time and length scales. This yields the system

$$\begin{aligned} \overline{u}_t &= D\nabla^2\overline{u} + \nu(\overline{u} + a\overline{v} - \overline{uv}^2 - C\overline{uv}) \\ \overline{v}_t &= \nabla^2\overline{v} + \nu(b\overline{v} + h\overline{u} + \overline{uv}^2 + C\overline{uv}), \end{aligned} \tag{3}$$

where the concentrations are scaled such that $(u, v) = \frac{1}{\sqrt{r_1}}(\overline{u}, \overline{v})$ and the time-space relation is given by $T = L^2/\delta$ ($t = T\tau$ and $x = L\overline{x}$). In the terms of the original parameters, the new parameters are $C = r_2/(\alpha\sqrt{r_1})$, $a = 1/\alpha$, $b = \beta/\alpha$, $h = \gamma/\alpha$ and $\nu = \alpha T$. The term C adjusts the relative strength of the quadratic and cubic nonlinearities favoring either stripe or spot selection.[39] From now on we omit the overlines for simplicity.

One can easily see that the system of Eq. (3) has a stationary state at $(u_c, v_c) = (0, 0)$. For $h \neq -1$ the system has also two other stationary states defined by $f(u_c, v_c) = g(u_c, v_c) = 0$ and they are given by

$$u_c^i = -v_c^i/K, \tag{4}$$

and

$$v_c^i = \frac{-C + (-1)^i \pm \sqrt{C^2 - 4(h - bK)}}{2} \tag{5}$$

where $K = \frac{1+h}{a+b}$ and $i = 1, 2$.

Linear analysis is a generally used method for evaluating the behavior of perturbations in a nonlinear system in the vicinity of a stationary state.[11,40,41] In the linear analysis one takes into account only the linear terms and thus the results are insufficient. However, within its limitations the method is typically quite efficient in predicting the existence of an instability and the characteristic wave length of it. The linearized system in the absence of diffusion can be written in the form $\vec{w}_t = \mathbf{A}\vec{w}$ and reads as

$$\begin{pmatrix} u_t \\ v_t \end{pmatrix} = \begin{pmatrix} f_u & f_v \\ g_u & g_v \end{pmatrix}_{u_c, v_c} \begin{pmatrix} u \\ v \end{pmatrix}, \tag{6}$$

where f_u, f_v, g_u and g_v in the matrix $\mathbf{A}$ denote the partial derivatives of the reaction kinetics evaluated at the stationary state (u_c, v_c). In the case of Eq. (3) the linearized matrix is given as

$$\mathbf{A} = \nu \begin{pmatrix} 1 - v_c^2 - Cv_c & -2u_c v_c + a - Cu_c \\ v_c^2 + h + Cv_c & b + 2u_c v_c + Cu_c \end{pmatrix}, \tag{7}$$

where u_c and v_c are given by Eqs. (4) and (5). In the linear analysis the spatial and time variance are taken into account by substituting a trial solution of the form $w(\vec{r}, t) = \sum_k c_k e^{\lambda t} w_k(\vec{r}, t)$ into the linearized system in the presence of diffusion. The eigenvalues of this linearized system are obtained from the equation

$$|\mathbf{A} - \mathbf{D}k^2 - \lambda \mathbf{I}| = 0, \tag{8}$$

where $\mathbf{A}$ is given by Eq. (6), $D_{11} = D_u$, $D_{22} = D_v$, $D_{12} = D_{21} = 0$ and $\mathbf{I}$ is the identity matrix in the general case. In the case of Eq. (3) $\mathbf{A}$ is given by Eq. (7), and $D_{11} = D$ and $D_{22} = 1$. The determinant in Eq. (8) can be solved, which yields the equation

$$\lambda^2 + \left[(D_u + D_v)k^2 - f_u - g_v\right]\lambda + D_u D_v k^4 - k^2(D_v f_u + D_u g_v) + f_u g_v - f_v g_u = 0, \tag{9}$$

where $k^2 = \vec{k} \cdot \vec{k}$. The dispersion relation $\lambda(k)$ predicting the unstable wave numbers can be solved from Eq. (9). One can obtain an estimate for the most unstable wave number and the critical value of the bifurcation parameter by considering the fact that at the onset of the instability $\lambda(k_c) = 0$. Thus the term independent of λ in Eq. (9) must be zero at k_c. In the case of the generic Turing model this condition reads as

$$Dk_c^4 - k_c^2 \nu(Db + 1) + \nu^2(b - ah) = 0. \tag{10}$$

At the onset this equation has only one solution given by $k_c^2 = \nu(Db + 1)/(2D)$, which takes place for the bifurcation parameter value $a = a_c = -(Db - 1)^2/(4Dh)$. An instability exists for $a < a_c$. The conditions for the Turing instability are widely known[8,11] to be the following

$$\begin{aligned} f_u + g_v &< 0 \\ f_u g_v - f_v g_u &> 0 \\ D_v f_u + D_u g_v &> 0. \end{aligned} \tag{11}$$

Based on linear analysis and numerical observations it can be deduced that for $h < -1$ stationary state $(0, 0)$ is no more unstable and one of the other stationary states shows a Hopf-like bifurcation to a damped time-dependent oscillatory state without a characteristic length scale. On the other hand, for $h > -1$ there is a coupling of Turing instability with a characteristic length (bifurcation of the state (0,0)) and a time-dependent instability with $k = 0$ unstable (bifurcation of the state defined by Eq. (5) with $i = 1$), which results in a transient large amplitude competition between oscillatory and fixed length scale instability. To simplify the

study of the generic model of Eq. (3), we will fix $h = -1$ from now on. This makes the $(0, 0)$ the only stationary state and simplifies our analysis.

In the case of the generic model with $h = -1$ the above conditions (Eq. (11)) and the previous reasoning yield the constraints $-b < a < a_c = (Db-1)^2/(4D)$ and $-1/D < b < -1$ for the Turing instability. Based on this one can sketch the stability diagram for the generic Turing model. This is presented in Fig. 1. From the stability diagram one can notice that the number of the parameter sets exhibiting Turing instability, i.e., the size of the Turing space (shaded region) is relatively small. For explanations of the other regions of the diagram see the caption.

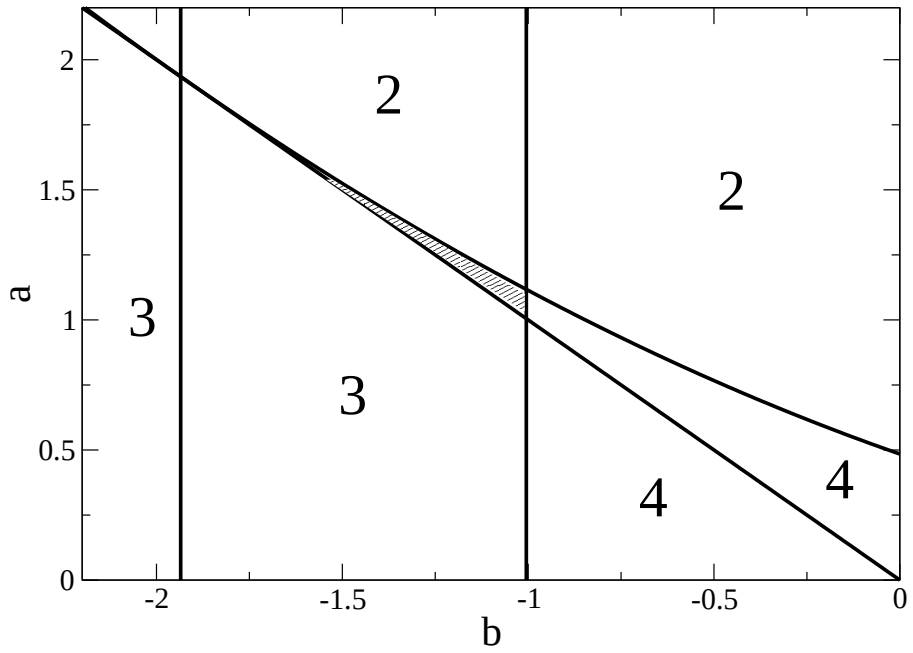

Fig. 1. The stability diagram of the generic Turing model (Eq. (3)). The Turing space (shaded region) is bounded by lines $b = -1/D$, $b = -1$, $b = -a$ and the curve $a = (Db-1)^2/(4D)$. For the plot parameters were fixed to $D = 0.516$. The other regions: stable state (2), other instabilities (3) and Hopf instability (4).

Based on the stability diagram one can choose parameters that result in the Turing instability. Here we use two sets of parameters that have been used earlier in the case of the generic Turing model.[39,42] For the non-dimensionalized generic model (with $L = 1$) the parameters are given as $D = 0.516$, $a = 1.112$, $b = -1.01$

and $\nu = 0.450$ for $k_c = 0.46$ ($a_c = 1.121$) and $D = 0.122$, $a = 2.513$, $b = -1.005$ and $\nu = 0.199$ for $k_c = 0.85$ ($a_c = 2.583$). The dispersion relation is obtained by solving Eq. (9) with respect to λ and plotting the real part of the solution. The dispersion relations corresponding to the onset of the instability (at $a = a_c$) and the above parameter sets resulting in the instability are shown in Fig. 2. The growing modes are of the form $Ae^{i\vec{k}\cdot\vec{r}}e^{\lambda(k)}$. Thus the wave numbers k with $Re\{\lambda(k)\} < 0$ will be damped, whereas the wave numbers with $Re\{\lambda(k)\} > 0$ will grow exponentially until the nonlinearities bound the growth. The dispersion relations in Fig. 2 tells us the growing modes and predicts the characteristic length of the pattern. The wave number and the wave length are related by $\lambda = 2\pi/k$.

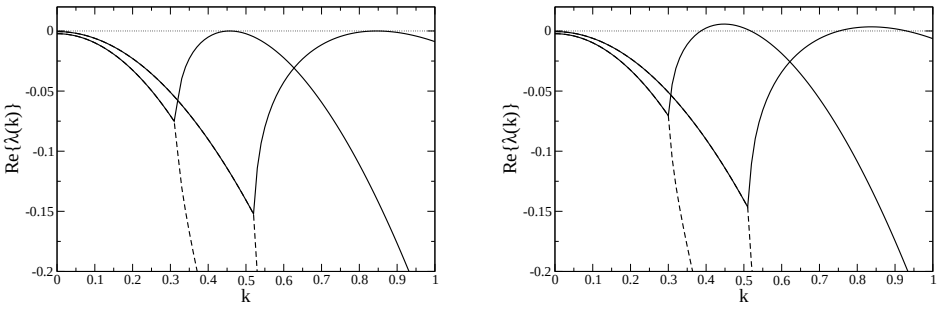

Fig. 2. The dispersion relations $\lambda(k)$ corresponding to two different parameter sets with $k_c = 0.46$ and $k_c = 0.85$, respectively. Left: At the onset of instability $a = a_c$ and there are no unstable modes. Right: For $a < a_c$ there is a finite wave length instability corresponding to wave numbers k for which $Re\{\lambda(k)\} > 0$.

Due to the width of the unstable wave window (Fig. 2), there is more than one unstable mode. The unstable modes that do not correspond to k_c, i.e., the highest point of the dispersion relation are called the sideband. The side band widens with the distance to onset $a_c - a$ as the bifurcation parameter a is varied. The linear analysis does not tell, which of these unstable modes will be chosen. In addition, there is degeneracy due to isotropy, i.e., there are many wave vector $\vec{k}$ having the same wave number $k = |\vec{k}|$. In a discrete three-dimensional system the wave number is given by

$$|\vec{k}| = 2\pi\sqrt{\left(\frac{n_x}{L_x}\right)^2 + \left(\frac{n_y}{L_y}\right)^2 + \left(\frac{n_z}{L_z}\right)^2}, \tag{12}$$

where $L_{x/y/z}$ denote the system size in respective directions and $n_{x/y/z}$ the respective wave number indices. For a one-dimensional system $n_y = n_z = 0$ and for a two-dimensional system $n_z = 0$. Based on Eq. (12) one notices that e.g. two-dimensional vectors $(k_c, 0)$, $(0, k_c)$ and $(k_c/\sqrt{2}, k_c/\sqrt{2})$ all correspond to the wave

number k_c and thus they are all simultaneously unstable. Actually, in a continuous system there would be an infinite number of unstable wave vectors pointing from the origin to the perimeter of a circle with a radius k_c. To tackle the problem of pattern selection, i.e., which of the degenarate modes will contribute to the final pattern a nonlinear analysis is required.

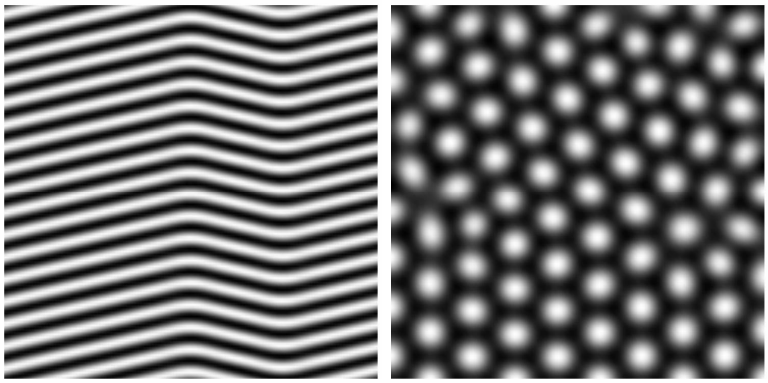

Fig. 3. Chemical concentration patterns obtained from numerical simulations of the Eq. (3) in a system sized 128×128. Left: Stripe pattern ($k_c = 0.85$, $C = 0$). Right: Hexagonal spotty pattern ($k_c = 0.46$, $C = 1.57$). See the text for the other parameters.

From the results of the linear analysis we can identify the parameter domain, which results in the Turing instability and approximate the characteristic wave length of the patterns. Fig. 3 shows a stripe pattern and a spotty pattern with different characteristic lengths obtained from a numerical simulation with different parameter values. These two morphologies are typical for reaction-diffusion systems in two dimensions.[43] The generic Turing model has been devised in such a way that by adjusting parameter C one can favor either stripe or spotty patterns.[39,42] The rigorous proof of this requires nonlinear bifurcation analysis and is the subject of the next section.

4. Nonlinear bifurcation theory

Bifurcation theory is a mathematical tool generally used for studying the dynamics of nonlinear systems.[44,45,46] The result of bifurcation analysis or weakly nonlinear analysis is a qualitative approximation for the changes in the dynamics of the system under study. In the case of Turing systems the bifurcation analysis answers the question concerning the changes in the stability of different simple morphologies as a parameter is varied. The bifurcation analysis has previously been applied in the cases of the Brysselator model[47] and the Lengyel-Epstein model[48]. The problem of these published analyses is that they omit the mathematical details required for understanding at an elementary level. In this section I will try to illustrate the idea

of bifurcation analysis and the related mathematical techniques in a meticulous manner.

The idea of the bifurcation analysis is to find a presentation for the concentration field $\vec{w} = (u, v)^T$ in terms of the active Fourier modes, i.e.,

$$\vec{w} = \vec{w_0} \sum_{\vec{k}_j} (W_j e^{i\vec{k}_j \cdot \vec{r}} + W_j^* e^{-i\vec{k}_j \cdot \vec{r}}), \tag{13}$$

where $\vec{w_0}$ defines the direction of the active modes. W_j and W_j^* are the amplitudes of the corresponding modes $\vec{k}_j$ and $-\vec{k}_j$. Notice that the sum of complex conjugates is real. The unstable modes have slow dynamics, whereas the stable modes relax quickly and are said to be slaved to the unstable modes. Typically the bifurcation analysis is carried out by observing changes as a function of the bifurcation parameter, i.e., the distance to onset. In the case of the generic Turing system (Eq. (3)) there is an additional quadratic nonlinearity, which is adjusted by parameter C. This parameter governs the morphology selection between linear (stripe) and radial (spot) structures instead of the bifurcation parameter and forces to some additional algebraic manipulations at the end of the bifurcation analysis.

The bifurcation analysis can be divided into three parts: derivation of the normal form for the amplitude equations in a particular symmetry, determining the parameters of the amplitude equations (there are various techniques for this) and finally analyzing the stability of different morphologies by applying the linear analysis (Sec. 3) on the system of amplitude equations. These three phases will be the respective topics of the following subsections.

4.1. *Derivation of the amplitude equations*

A system of n amplitude equations describes the time variation of the amplitudes W_j of the unstable modes $\vec{k}_j$ $(j = 1, \ldots, n)$. The amplitude equations contain a linear part corresponding to the linear growth predicted by the positive eigenvalue of the linearized system defined by Eq. (9) and a nonlinear part due to nonlinear coupling of the unstable modes. Thus the most general form of an amplitude equation given by

$$\frac{dW_j}{dt} = \lambda_c W_j + f_j(W_1, \ldots, W_n). \tag{14}$$

The eigenvalue may be approximated in the vicinity of the onset by a linear approximation defined by

$$\lambda_c = \left.\frac{d\lambda}{da}\right|_{a=a_c} (a - a_c) = \frac{\nu^2(\nu - 2R)}{(\nu(1+b) - 2R)(\nu - R)}, \tag{15}$$

where $R = \nu(Db + 1)/2$ with notations of the generic Turing model (Eq. (3)). The exact form of the term $f(W_1, \ldots, W_n)$ in Eq. (14) depends on the symmetries under study and may be constructed by geometrical arguments. In two dimensions reaction-diffusion systems typically exhibit either stripes or a hexagonally arranged

spots (Fig. 3). Thus the natural selection for the study of 2D patterns is a hexagonal lattice. In three dimensions there are various possibilities: One can study the simple cubic lattice (SC), base-centered cubic lattice (BCC) or face-centered cubic lattice (FCC).[49] Callahan and Knobloch have been among the first to address the problem of bifurcations in three-dimensional Turing systems.[50,51,52] In the following we will derive the amplitude equations for the two-dimensional hexagonal lattice and three-dimensional SC- and BCC-lattices.

2D hexagonal lattice

The base vectors of a two-dimensional hexagonal lattice can be chosen to be $\vec{k}_1 = k_c(1,0)$, $\vec{k}_2 = k_c(-1/2, \sqrt{3}/2)$ and $\vec{k}_3 = k_c(-1/2, -\sqrt{3}/2)$ with $|\vec{k}_{1,2,3}| = k_c$. Since $-\vec{k}_1 - \vec{k}_2 = \vec{k}_3$ we can say that a hexagonal lattice exhibits resonant modes, which one must take into account, while deriving the form of the amplitude equations. In a simple square lattice there would not be any resonant modes, since any subset of the base vectors does not sum into another base vector. The base vectors of a hexagonal lattice and the idea of resonant modes is illustrated in Fig. 4.

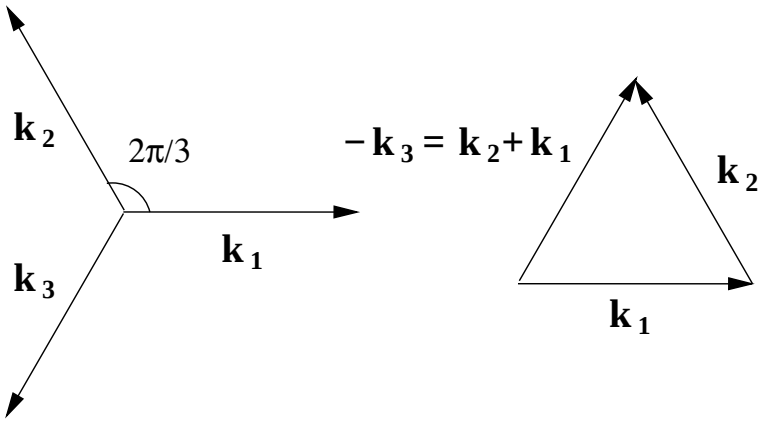

Fig. 4. The base vectors of a two-dimensional hexagonal lattice are not linearly independent and thus there are resonant modes.

Based on the above reasoning one would suggest that there must be a quadratic coupling term in the amplitude equation: Since the negative sum of two other modes may contribute to any one mode, there must be a term of the form $(-W_{j+1}^*)(-W_{j+2}^*)$ in $f_j(W_1, W_2, W_3)$ $(j = 1, 2, 3\,(mod\,3))$. The other combinations of wave vectors that sum up to $\vec{k}_j$ are $\vec{k}_j - \vec{k}_j + \vec{k}_j$, $\vec{k}_{j+1} - \vec{k}_{j+1} + \vec{k}_j$, and $\vec{k}_{j+2} - \vec{k}_{j+2} + \vec{k}_j$. The respective contributions to $f_j(W_1, W_2, W_3)$ are $-|W_j|^2 W_j$, $-|W_{j+1}|^2 W_j$ and $-|W_{j+2}|^2 W_j$. We assume that the saturation occurs at the third order and thus take into account only the sums of maximum three vectors. Now the full amplitude equation for the

two-dimensional hexagonal lattice may be written as

$$\frac{dW_j}{dt} = \lambda_c W_j + \Gamma W^*_{j+1} W^*_{j+2} - g[|W_j|^2 + \kappa(|W_{j+1}|^2 + |W_{j+2}|^2)]W_j, \qquad (16)$$

where the coefficients Γ, g and κ can be presented in terms of the parameters of the original reaction-diffusion system (Eq. (3)). The coefficients are obtained via complicated mathematical techniques, which will be discussed in the next subsection.

3D SC-lattice

The base vectors of a three-dimensional simple cubic lattice can be chosen to be $\vec{k}_1 = k_c(1,0,0)$, $\vec{k}_2 = k_c(0,1,0)$ and $\vec{k}_3 = k_c(0,0,1)$ with $|\vec{k}_{1,2,3}| = k_c$. Now the base vectors are linearly independent and thus there are no resonant modes. By following the same reasoning as in the case of 2D hexagonal lattice, one can deduce the form of the amplitude equations to be the following

$$\frac{dW_j}{dt} = \lambda_c W_j - g[|W_j|^2 + \kappa(|W_{j+1}|^2 + |W_{j+2}|^2)]W_j. \qquad (17)$$

3D BCC-lattice

The three-dimensional base-centered cubic lattice is a little bit more tricky. The set of base vectors is $\vec{k}_1 = k_c(1,1,1)/\sqrt{3}$, $\vec{k}_2 = k_c(1,1,-1)/\sqrt{3}$, $\vec{k}_3 = k_c(1,-1,1)/\sqrt{3}$ and $\vec{k}_4 = k_c(1,-1,-1)/\sqrt{3}$ with $|\vec{k}_{1,2,3,4}| = k_c$. These are not linearly independent since e.g. $\vec{k}_2 + \vec{k}_3 - \vec{k}_4 = \vec{k}_1$. Thus there is a cubic resonant coupling term and in addition there are the other nonlinear terms. The amplitude equations are given by

$$\frac{dW_j}{dt} = \lambda_c W_j + \Gamma W^*_{j+1} W^*_{j+2} W^*_{j+3} - g[|W_j|^2 + \kappa(|W_{j+1}|^2 + |W_{j+2}|^2 + |W_{j+3}|^2)]W_j, \qquad (18)$$

where $(j = 1, 2, 3, 4\ (mod\ 4))$.

4.2. *Center manifold reduction*

There are various methods for determining the parameters for the amplitude equation. In the most used method, the multiscale expansion,[44,47] the bifurcation parameter and the chemical concentrations are expanded in a small parameter (e.g. $a - a_c = \epsilon a_1 + \epsilon^2 a_2 + ...$) and the coefficients are obtained based on the solvability conditions of the resulting linear differential equations at different degrees of ϵ. In this article we will not use multiscale expansion, but a related method called the center manifold reduction[45,52]. We will take the method of center manifold reduction as given and for the mathematical justification of it we refer the reader elsewhere.[45,51,53]

The purpose of the center manifold reduction is to devise a mapping from the concentration space (Eq. (3)) to a high-dimensional equivariant amplitude space (Eq. (14)). The center manifold is a surface separating the unstable and stable

manifolds in the wave vector space. The center manifold reduction confines the nonlinear effects in the system to the center manifold and thus one can obtain good approximations for the stability of different structures. In the following, we will sketch the general procedure to obtain the amplitude equations following Callahan and Knobloch[52] to whom we refer the reader for details.

In general, we can write the component h of a Turing system with n chemical species ($h \in \{1, ..., n\}$) as

$$\frac{dX^h}{dt} = D^h \nabla^2 W^h + \sum_{i=1}^{n} A^{h,i} W^i + \sum_{i=1}^{n}\sum_{j=1}^{n} A^{h,ij} X^i X^j + \sum_{i=1}^{n}\sum_{j=1}^{n}\sum_{k=1}^{n} A^{h,ijk} X^i X^j X^k + ... \tag{19}$$

where $X^h = X^h(\vec{x}, t)$ is the spatially varying concentration of one chemical species and $X^h = 0$ in the uniform stationary state. The tensors $A^{h,i}$, $A^{h,ij}$ and $A^{h,ijk}$ define the parameters for the component h and are symmetric with respect to permutations of the indices. In a discrete system we can write the concentration in a certain position of the lattice as

$$X^h(\vec{x}, t) = \sum_{l \in L} \tilde{X}_l^h(t) e^{i\vec{k}_l \cdot l}, \tag{20}$$

where L is the set of all lattice points. From now on we write species indices (e.g. h) as superscripts and lattice point indices (e.g. l) as subscripts. Substituting Eq. (20) into Eq. (19) yields

$$\frac{dX_l^h}{dt} = -D^h |\vec{k}_l|^2 X_l^h + A^{h,i} X_l^i + A^{h,ij} \sum_{l_1+l_2=l} X_{l_1}^i X_{l_2}^j + A^{h,ijk} \sum_{l_1+l_2+l_3=l} X_{l_1}^i X_{l_2}^j X_{l_3}^k, \tag{21}$$

where we have used the Einstein summation convention for the indices i, j and k, and included only the terms up to cubic order. The linear part the previous equation defines the unstable modes (see Sec. 3) and the linear matrix can be written in the form

$$J_l^{h,i} = -D^h k_l^2 \delta^{h,i} + A^{h,i}, \tag{22}$$

where it is assumed that there is no cross-diffusion ($\delta^{h,i} = 1$ only when $h = i$). For each lattice point we may now choose a matrix

$$S_l = \begin{pmatrix} \alpha_l^{11} & \dots & \alpha_l^{1n} \\ \vdots & \ddots & \vdots \\ \alpha_l^{n1} & \dots & \alpha_l^{nn} \end{pmatrix}, \tag{23}$$

with $det(\mathbf{S}_l) = 1$. In addition, we require that it has an inverse matrix $S_l^{-1} = \{\beta_l^{ij}\}$ such that

$$S_l^{-1} J_l S_l = \begin{pmatrix} \lambda_l^1 & & \\ & \ddots & \\ & & \lambda_l^n \end{pmatrix}. \tag{24}$$

The conditions for this similarity transformation are widely known.[52,54] Now we can map the original concentrations (Eq. (21)) to a new basis defined by $S_l^{-1}X_l = W_l$. In this new basis Eq. (21) reads as

$$\frac{dW_l^g}{dt} = \lambda_l^g W_l^g + \beta_l^{gh} A^{h,ij} \sum_{l_1+l_2=l} \alpha_{l_1}^{ii'} W_{l_1}^{i'} \alpha_{l_2}^{jj'} W_{l_2}^{j'} + \beta_l^{gh} A^{h,ijk} \sum_{l_1+l_2+l_3=l} \alpha_{l_1}^{ii'} W_{l_1}^{i'} \alpha_{l_2}^{jj'} W_{l_2}^{j'} \alpha_{l_3}^{kk'} W_{l_3}^{k'}. \quad (25)$$

The coefficient of the linear term is defined by Eq. (15). The coefficients of the nonlinear terms can be calculated at the onset by fixing $a = a_c$ and using the information about stable and unstable modes. Using the fact that the only contribution to the growth of the stable modes comes via a nonlinear coupling, one can derive relations for the parameters.[52] Further simplification of Eq. (25) for a critical wave vector m at the onset ($\lambda_l^g = 0$) yields

$$\frac{dW_m^1}{dt} = \beta^{1h} A^{h,ij} \alpha^{i1} \alpha^{j1} \sum_{m_1+m_2=m} W_{m_1}^1 W_{m_2}^1 + \sum_{m_1+m_2+m_3=m} F(m_2+m_3) W_{m_1}^1 W_{m_2}^1 W_{m_3}^1, \quad (26)$$

where

$$F(r) \equiv -2\beta^{1h} A^{h,ij} \alpha^{i1} (J_r^{-1})^{ja} A^{a,bc} \alpha^{b1} \alpha^{c1} + \beta^{1h} A^{h,ijk} \alpha^{i1} \alpha^{j1} \alpha^{k1}. \quad (27)$$

One should notice that the coefficient $F(r)$ depends on the argument r only through the square of its length. Thus the previous treatment has been general and not specific to any particular symmetry. In the following, we will derive the form of the function $F(r)$ for three different lattices in two or three dimensions. In order to survive the horrendous linear algebra involved in the calculation, we follow a computation procedure that has been used earlier.[52] The derivation is based on finding the number and type of resonant modes that contribute to the amplitude of a particular mode as shown in Eq. (26). Due to symmetry, the coefficient of all the amplitude equations in a particular amplitude system (Eq. (16) or (17) or (18)) are the same.

2D hexagonal lattice

In the hexagonal lattice two wave vectors sum up to another wave vector. The base vectors for the hexagonal lattice are given by $\vec{k}_1 = (1, 0)$, $\vec{k}_2 = (-1/2, \sqrt{3}/2)$ and $\vec{k}_3 = (-1/2, -\sqrt{3}/2)$. The strength of the quadratic coupling term is determined by the first term in Eq. (26). Since there are two possible selections (permutations) of m_1 and m_2, i.e., $-\vec{k}_3 - \vec{k}_2 = -\vec{k}_2 - \vec{k}_3 = \vec{k}_1$ one has to take into account both of them. Thus the quadratic coupling parameter in Eq. (16) is given by $\Gamma = 2\beta^{1h} A^{h,ij} \alpha^{i1} \alpha^{j1}$. The strength of the cubic coupling terms can be found by similar

arguments. However, there are two cases that have to be treated separately, case 1: $m_1 = m_2 \neq m_3$ and case 2: $m_1 = m_2 = m_3$.

In the first case the coupling is of the type $k_1 + k_2 - k_2 = k_1$. There are three different combinations of m_2 and m_3 with two corresponding permutations. The combinations are

(1) $m_2 = k_2$ and $m_3 = -k_2$ with $|m_2 + m_3|^2 = 0$,
(2) $m_2 = k_1$ and $m_3 = k_2$ with $|m_2 + m_3|^2 = 1$,
(3) $m_2 = k_1$ and $m_3 = -k_2$ with $|m_2 + m_3|^2 = 3$,

which defines the coefficient $g\kappa$ in Eq. (16) to have the value $g\kappa = -2F(0) - 2F(1) - 2F(3)$.

In the second case the coupling is of the type $k_1 + k_1 - k_1 = k_1$. There are three possible permutations with

(1) $m_2 = k_1$ and $m_3 = -k_1$ with $|m_2 + m_3|^2 = 0$,
(2) $m_2 = -k_1$ and $m_3 = k_1$ with $|m_2 + m_3|^2 = 0$,
(3) $m_2 = k_1$ and $m_3 = k_1$ with $|m_2 + m_3|^2 = 4$,

which results in $g = -2F(0) - F(4)$ for Eq. (16).

Based on the above reasoning and Eq. (27) one may calculate the exact form of the coefficient in Eq. (16) with respect to the parameters of the generic Turing model of Eq. (3). The parameters of the amplitude equations are given by

$$\Gamma = \frac{-2bC\nu R\sqrt{\nu(\nu - 2R)}}{(\nu + b\nu - 2R)\sqrt{(\nu + b\nu - 2R)(\nu - R)}}, \tag{28}$$

$$g = \frac{3b\nu^2(\nu - 2R)R}{(\nu + b\nu - 2R)^2(\nu - R)}, \tag{29}$$

$$\kappa = 2, \tag{30}$$

where we have denoted $R = Dk_c^2 = \nu(Db + 1)/2$. The linear coefficient of Eq. (16) is given by Eq. (15).

3D SC-lattice

In the SC-lattice the base vectors are independent and given as $\vec{k}_1 = (1, 0, 0)$, $\vec{k}_2 = (0, 1, 0)$ and $\vec{k}_3 = (0, 0, 1)$. There are no resonant modes. Following the ideas above in the first case we find

(1) $m_2 = k_2$ and $m_3 = -k_2$ with $|m_2 + m_3|^2 = 0$,
(2) $m_2 = k_1$ and $m_3 = k_2$ with $|m_2 + m_3|^2 = 2$,
(3) $m_2 = k_1$ and $m_3 = -k_2$ with $|m_2 + m_3|^2 = 2$,

which defines the coefficient $g\kappa = -2F(0) - 4F(2)$ in Eq. (16). The second case yields the permutations

(1) $m_2 = k_1$ and $m_3 = -k_1$ with $|m_2 + m_3|^2 = 0$,

(2) $m_2 = -k_1$ and $m_3 = k_1$ with $|m_2 + m_3|^2 = 0$,
(3) $m_2 = k_1$ and $m_3 = k_1$ with $|m_2 + m_3|^2 = 4$,

which gives $g = -2F(0) - F(4)$ for Eq. (16).

For the amplitude equations of the three-dimensional SC-lattice (Eq. (17)) the coefficients are given by

$$g = \frac{-b\nu^2(C^2(8\nu - 23R) - 27R)(\nu - 2R)}{9(\nu + b\nu - 2R)^2(\nu - R)}, \tag{31}$$

$$\kappa = \frac{18(C^2(8\nu - 7R) - 3R)}{C^2(8\nu - 23R) - 27R}, \tag{32}$$

where we have again denoted $R = Dk_c^2 = \nu(Db + 1)/2$ and the linear coefficient of Eq. (17) is given by Eq. (15).

3D BCC-lattice

In the BCC-lattice the base vectors given by $\vec{k}_1 = (1, 1, 1)/\sqrt{3}$, $\vec{k}_2 = (1, 1, -1)/\sqrt{3}$, $\vec{k}_3 = (1, -1, 1)/\sqrt{3}$ and $\vec{k}_4 = (1, -1, -1)/\sqrt{3}$ are not linearly independent. To find the coefficient of the resonant contribution to Eq. (18) one must considers the possible combinations of the two last terms within the sum $k_2 + k_3 - k_4 = k_1$. These are given by

(1) $m_2 = k_3$ and $m_3 = -k_4$ with $|m_2 + m_3|^2 = \frac{4}{3}$,
(2) $m_2 = -k_4$ and $m_3 = k_2$ with $|m_2 + m_3|^2 = \frac{4}{3}$,
(3) $m_2 = k_2$ and $m_3 = k_3$ with $|m_2 + m_3|^2 = \frac{4}{3}$,

which yields the resonant coupling coefficient $\Gamma = 6F(\frac{4}{3})$ for the Eq. (18).

The two other coefficient are determined using the same reasoning as above. In the first case one gets

(1) $m_2 = k_2$ and $m_3 = -k_2$ with $|m_2 + m_3|^2 = 0$,
(2) $m_2 = k_1$ and $m_3 = -k_2$ with $|m_2 + m_3|^2 = \frac{4}{3}$,
(3) $m_2 = k_1$ and $m_3 = k_2$ with $|m_2 + m_3|^2 = \frac{8}{3}$,

which results in the coefficient $g\kappa = -2F(0) - 2F(\frac{4}{3}) - 2F(\frac{8}{3})$ for the Eq. (18). In the second case we get the permutations

(1) $m_2 = k_1$ and $m_3 = -k_1$ with $|m_2 + m_3|^2 = 0$,
(2) $m_2 = -k_1$ and $m_3 = k_1$ with $|m_2 + m_3|^2 = 0$,
(3) $m_2 = k_1$ and $m_3 = k_1$ with $|m_2 + m_3|^2 = 4$,

which yields $g = -2F(0) - F(4)$ for the Eq. (18).

The coefficients of the amplitude equations of the three-dimensional BCC-lattice (Eq. (18)) can be written as

$$\Gamma = \frac{6b\nu^2(\nu - 2R)(3C^2(8\nu - 7R) - R)}{(\nu + b\nu - 2R)^2(\nu - R)}, \tag{33}$$

$$g = \frac{-b\nu^2(C^2(8\nu - 23R) - 27R)(\nu - 2R)}{9(\nu + b\nu - 2R)^2(\nu - R)}, \tag{34}$$

$$\kappa = \frac{18(C^2(648\nu - 583R) - 75R)}{25(C^2(8\nu - 23R) - 27R)}, \tag{35}$$

where $R = \nu(Db+1)/2$ and the linear coefficient λ_c of Eq. (18) is defined by Eq. (15).

4.3. *Stability of different structures*

After we have obtained the system of coupled amplitude equations written with respect to the parameters of the original reaction-diffusion equations, we may now employ linear analysis to study the amplitudes. First one has to determine the stationary states W_c of the amplitude system, which depends on the symmetry under study (Eq. (16), (17) or (18)). After that one can linearize the system (as in Eq. (6)) and construct the corresponding Jacobian linear matrix $\mathbf{A}$, which is determined by

$$\{\mathbf{A}\}_{ij} = \left| \frac{df_i}{d|W_j|} \right|_{(W_1^c, W_2^c, W_3^c)}, \tag{36}$$

where f_i denotes the right-hand side of the corresponding amplitude equation i and the element is evaluated at the stationary state $W_c = (W_1^c, W_2^c, W_3^c)$. Based on this one can plot the bifurcation diagram, i.e., the eigenvalues of the linearized system $dW/dt = \mathbf{A}W$ as a function of the parameter C in Eq. (3), which contributes to the morphology selection in the generic Turing model. The parameters of the generic Turing model that we have used in the analysis presented here correspond to the mode $k_c = 0.85$ (see Fig. 2).

2D hexagonal lattice

In the case of two-dimensional patterns we are interested in the stability of stripes ($W_c = (W_1^c, 0, 0)^T$) and hexagonally arranged spots ($W_c = (W_1^c, W_2^c, W_3^c)^T$ with $W_1^c = W_2^c = W_3^c$). For the stability analysis of rhombic patterns and anisotropic mixed amplitude states we refer the reader elsewhere.[55] The system of amplitude equations for a two-dimensional hexagonal lattice can be written based on Eq. (16) as

$$\begin{aligned}
\frac{dW_1}{dt} &= \lambda_c W_1 + \Gamma W_2^* W_3^* - g[|W_1|^2 + \kappa(|W_2|^2 + |W_3|^2)]W_1, \\
\frac{dW_2}{dt} &= \lambda_c W_2 + \Gamma W_1^* W_3^* - g[|W_2|^2 + \kappa(|W_1|^2 + |W_3|^2)]W_2, \\
\frac{dW_3}{dt} &= \lambda_c W_3 + \Gamma W_1^* W_2^* - g[|W_3|^2 + \kappa(|W_1|^2 + |W_2|^2)]W_3,
\end{aligned} \tag{37}$$

where the coefficients λ_c, Γ, g and κ are given by Eqs. (15), (28), (29) and (30), respectively. In the case of stripes $W_2^c = W_3^c = 0$ and the system reduces to only one equation. Now the stationary states defined by the zeros of the right-hand side of Eqs. (37) can easily be shown to be $W_1^c = \sqrt{\frac{\lambda_c}{g}} e^{i\phi_1}$. In the case of hexagonal spots we have three equations and by choosing a solution such that $W_c = W_1^c = W_2^c = W_3^c$ we obtain the two stationary states defined by

$$|W_\pm^c| = \frac{|\Gamma| \pm \sqrt{\Gamma^2 + 4\lambda_c g[1+2\kappa]}}{2g(1+2\kappa)}. \tag{38}$$

In the case of stripes the eigenvalues of the linearized matrix (Eq. (36)) are given as $\mu_1^s = -2\lambda_c$, $\mu_2^s = -\Gamma\sqrt{\frac{\lambda_c}{g}} + \lambda_c(1-\kappa)$ and $\mu_3^s = \Gamma\sqrt{\frac{\lambda_c}{g}} + \lambda_c(1-\kappa)$. Noticing that $\mu_1^s < 0$ and $\mu_3^s > \mu_2$ follows that the stability of stripes is determined by the sign of μ_3^s. The stripes are unstable for $\mu_3^s > 0$ and stable for $\mu_3^s < 0$.

In the case of the hexagonally arranged spots the eigenvalues of the system are given as $\mu_{1,2}^h = \lambda_c - W_c^\pm(\Gamma + 3gW_c^\pm)$ and $\mu_3^h = \lambda_c + W_c^\pm(2\Gamma - 3g(2\kappa+1)W_c^\pm)$, where $W_c^\pm$ is defined by Eq. (38). Since there are two stationary states corresponding to hexagonal symmetry one must analyze the stability of both of them. For stability all the eigenvalues must be negative, i.e., $\mu_{1,2}^h < 0$ and $\mu_3^h < 0$. After writing the eigenvalues in terms of the original parameters (Eqs. (15), (28), (29), (30)) one can plot the eigenvalues as a function of the nonlinear coefficient C, which is known to adjust the competition between stripes and spots.[39] The result is shown in Fig. 5, from where one can determine the parameter regimes for which a given pattern is stable, i.e., $\mu(C) < 0$.

Fig. 5 implies that the hexagonal branch corresponding to W_c^+ is always unstable. Thus there is only one isotropic hexagonal solution to the equations that is stable within certain parameter regime. The analysis predicts that stripes are stable for $C < 0.161$ while using the parameters of mode $k_c = 0.85$. On the other hand, the other hexagonal branch is predicted to be stable for $0.084 < C < 0.611$. The most important information obtained from Fig. 5 is the region of bistability, which is predicted to be between $0.084 < C < 0.161$. Since the bifurcation analysis is based on weakly nonlinear approximation of the dynamics, it can be expected that it fails, when a strong nonlinear action is present. For example, based on the result of the numerical simulation presented in Fig. 3 one can see that the hexagonal spot pattern exists for $C = 1.57$. The bifurcation analysis, however, predicts that hexagons are unstable for all $C > 0.611$. This discrepancy is due to the approximations of the bifurcation theory, which hold only for weak nonlinearities.

3D SC-lattice

In the case of three-dimensional simple cubic lattice there are three possibilities for the structure. One may get planar structures ($W_c = (W_1^c, 0, 0)^T$), cylindrical structures ($W_c = (W_1^c, W_2^c, 0)^T$) or spherical droplet structures ($W_c = (W_1^c, W_2^c, W_3^c)^T$).

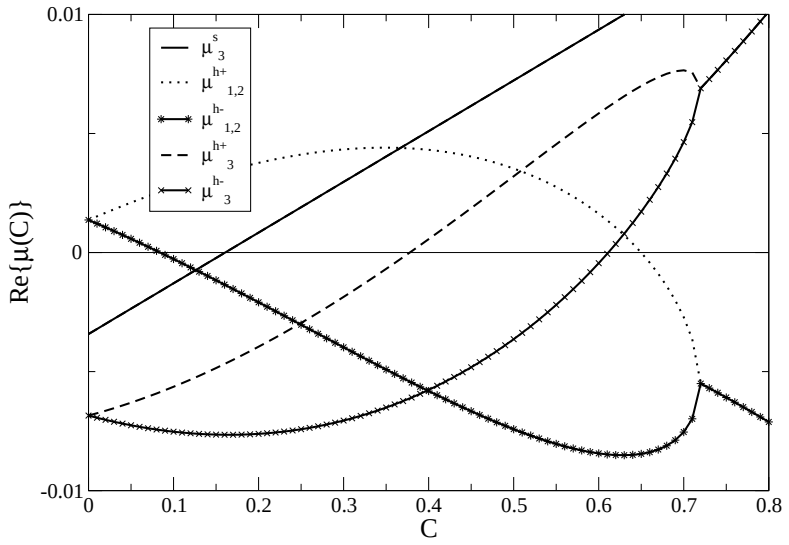

Fig. 5. The real part of the eigenvalues $\mu(C)$ of the linearized amplitude system of the two-dimensional hexagonal symmetry as a function of the parameter C. Eigenvalue μ_3^s determines the stability of the stripes, $\mu_{1,2}^{h+}$ and μ_3^{h+} determine the stability of one hexagonal branch, and $\mu_{1,2}^{h-}$ and μ_3^{h-} determine the stability of the other hexagonal branch. The morphology is stable if the corresponding $\mu(C) < 0$.

The amplitude equations of a three-dimensional SC-lattice are based on Eq. (17) and the system is given as

$$\begin{aligned}
\frac{dW_1}{dt} &= \lambda_c W_1 - g[|W_1|^2 + \kappa(|W_2|^2 + |W_3|^2)]W_1, \\
\frac{dW_2}{dt} &= \lambda_c W_2 - g[|W_2|^2 + \kappa(|W_1|^2 + |W_3|^2)]W_2, \\
\frac{dW_3}{dt} &= \lambda_c W_3 - g[|W_3|^2 + \kappa(|W_1|^2 + |W_2|^2)]W_3,
\end{aligned} \tag{39}$$

where the coefficients λ_c, g and κ are given by Eqs. (15), (31) and (32), respectively.

The stationary state corresponding to the planar lamellae is given as $|W_1^c| = \sqrt{\frac{\lambda_c}{g}}$. For the cylindrical structure we get $|W_1^c| = |W_2^c| = \sqrt{\frac{\lambda_c}{g(\kappa+1)}}$ and for the isotropic stationary state of SC-droplets $|W_1^c| = |W_2^c| = |W_3^c| = \sqrt{\frac{\lambda_c}{g(2\kappa+1)}}$. In the case of planar lamellae the eigenvalues of the linearized matrix (Eq. (36)) are given by $\mu_1^{Lam} = -2\lambda_c$ and $\mu_{2,3}^{Lam} = \lambda_c(1-\kappa)$. Noticing that $\mu_1^{Lam} < 0$ follows that the stability of the planar structures is determined by $\mu_{2,3}^{Lam}$. Repeating the same treatment for the cylindrical structures we find that the real part of the dominant

eigenvalue is $\mu_{2,3}^{Cyl} = \lambda_c - 3gW_c^2$. For the SC-droplets the stability determining eigenvalue is given by $\mu_{2,3}^{Sc} = \lambda_c - 3gW_c^2$. The real parts of the eigenvalues are presented in Fig. 6.

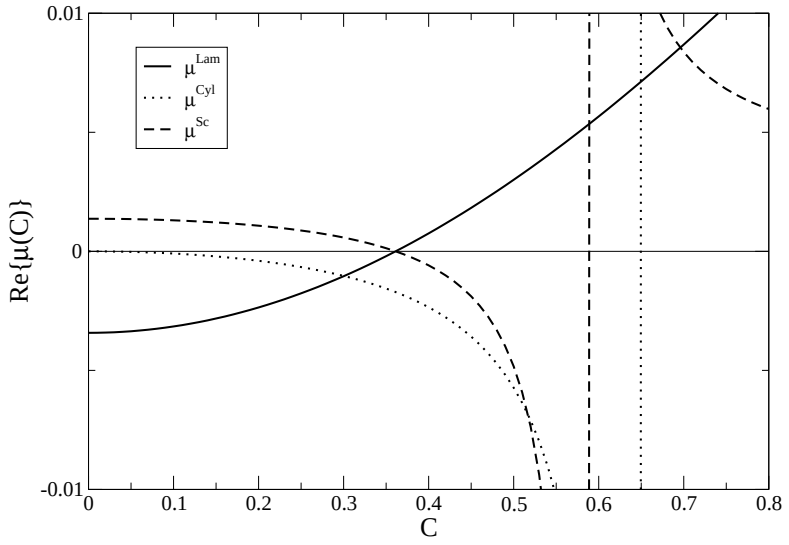

Fig. 6. The real part of the eigenvalues $\mu(C)$ of the linearized amplitude system of the three-dimensional SC-lattice as a function of the parameter C. Eigenvalue μ^{Lam} determines the stability of the planar lamellae, μ^{Cyl} determines the stability of cylindrical structures, and μ^{Sc} determines the stability of the spherical droplets organized in a SC-lattice. The morphology is stable if the corresponding $\mu(C) < 0$.

Based on Fig. 6 it can be reasoned that the bifurcation analysis does not predict a bistability between planes and spherical shapes in three dimensions, but the stability of those structures is exclusive. The planes are predicted to be stable for $C < 0.361$ and the spherical shapes stable for $0.361 < C < 0.589$. The square packed cylinders, however, are predicted to be stable for all $C < 0.650$. It can again be noticed that the bifurcation analysis fails for strong nonlinear interaction, i.e., high values of parameter C.

3D BCC-lattice

In the case of three-dimensional BCC-lattice there are numerous possibilities for the structure.[52] Here we analyze only the stability of lamellar structures ($W_c = (W_1^c, 0, 0, 0)^T$) and spherical droplets organized in a BCC-lattice ($W_c =$

$(W_1^c, W_2^c, W_3^c, W_4^c)^T$). The amplitude equations of a three-dimensional BCC-lattice are defined by Eq. (18) and the system is given by

$$\begin{aligned}
\frac{dW_1}{dt} &= \lambda_c W_1 + \Gamma W_2^* W_3^* W_4^* - g[|W_1|^2 + \kappa(|W_2|^2 + |W_3|^2) + |W_4|^2)]W_1, \\
\frac{dW_2}{dt} &= \lambda_c W_2 + \Gamma W_1^* W_3^* W_4^* - g[|W_2|^2 + \kappa(|W_1|^2 + |W_3|^2) + |W_4|^2)]W_2, \\
\frac{dW_3}{dt} &= \lambda_c W_3 + \Gamma W_1^* W_2^* W_4^* - g[|W_3|^2 + \kappa(|W_1|^2 + |W_2|^2) + |W_4|^2)]W_3, \\
\frac{dW_4}{dt} &= \lambda_c W_4 + \Gamma W_1^* W_2^* W_3^* - g[|W_4|^2 + \kappa(|W_1|^2 + |W_2|^2) + |W_3|^2)]W_4, \quad (40)
\end{aligned}$$

where the coefficients λ_c, Γ, g and κ are given by Eqs. (15), (33), (34) and (35), respectively.

The stationary state corresponding to planar lamellae is defined by $|W_1^c| = \sqrt{\frac{\lambda_c}{g}}$, with $|W_2^c| = |W_3^c| = |W_4^c| = 0$. For the stationary state of BCC-droplets with constraint $|W_1^c| = |W_2^c| = |W_3^c| = |W_4^c|$ we get $|W_i^c| = \sqrt{\frac{\lambda_c}{g(3\kappa+1)-\Gamma}}$. For planar lamellae the eigenvalues of the linearized matrix (Eq. (36)) are given by $\mu_1^{Lam} = -2\lambda_c$ and $\mu_{2,3,4}^{Lam} = \lambda_c(1-\kappa)$. Noticing that $\mu_1^{Lam} < 0$ follows that the stability of the planar structures is again determined by $\mu_{2,3,4}^{Lam}$. For the BCC-droplets, on the other hand, the stability determining eigenvalue is given by $\mu_{2,3,4}^{Sc} = \lambda_c - 3(\Gamma + g(K + 3))W_c^2$. The real parts of these eigenvalues are presented in Fig. 7 as a function of C.

From Fig. 7 one can see that there is a bistability between planes and BCC droplet structures for $0.181 < C < 0.204$. The planes are predicted to be stable for $C < 0.204$ and the spherical shapes stable for $0.181 < C < 0.255$. It can again be observed that the bifurcation analysis fails already at a reasonable low nonlinear interaction predicting that the spherical structures become unstable at $C < 0.255$. The stability of the other possible structures in BCC-lattice remains to be studied in the case of the generic Turing model.

5. Conclusions

Turing pattern formation is nowadays of great interest. The observation of real chemical patterns some 14 years ago confirmed that the theoretical ideas hypotetized by Alan Turing almost 40 years earlier were not only mathematical formulations, but a pioneering contribution to the theory of nonlinear dynamics. The contribution of Alan Turing to bioinformation technology and biology still remains controversial, although Turing models have been shown to be able to imitate many biological patterns found on animals[11,13,56], skeptics argue that more evidence is needed and the exact morphogens that behave according to Turing mechanism have to be named based on experimental studies by developmental biologists. However, there is a seed of truth in the cautiousness, since a numerical Turing model has even been shown to be able to exhibit patterns resembling the letters of alphabet if some heavy

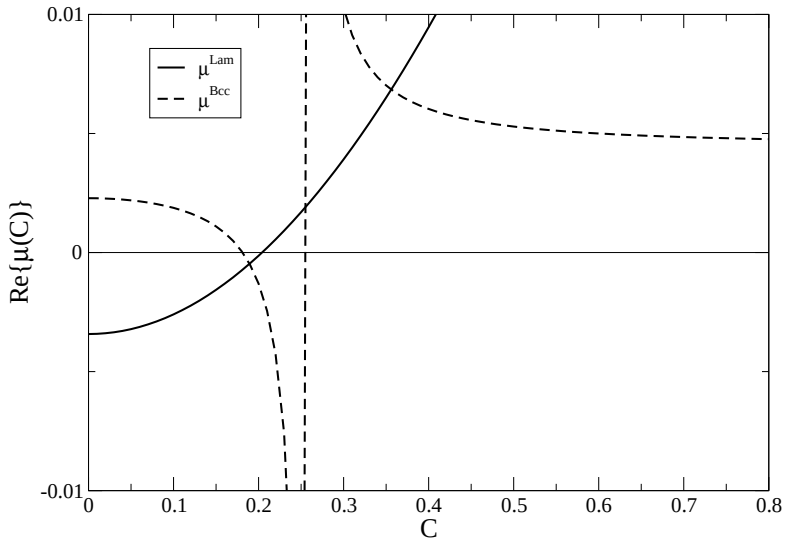

Fig. 7. The real part of the eigenvalues $\mu(C)$ of the linearized amplitude system of the three-dimensional BCC-lattice as a function of the parameter C. Eigenvalue μ^{Lam} determines the stability of the planar lamellae and μ^{Bcc} determines the stability of the spherical droplets organized in a BCC-lattice. The morphology is stable if the corresponding $\mu(C) < 0$.

manipulation of the dynamics is carried out.[57]

Irrespective of the biological relevance of the Turing systems, they are also of great interest from the physicists' point of view. Nowadays symmetry-breaking and self-organization are all in a day's work for physicists and the knowledge of other fields of physics may be applied to Turing systems and vice versa. The difficulty is, however, that making fundamental theoretical contributions to the theory of Turing pattern formation seems to be a penultimate challenge and thus most of the work in the field relies at least in part on experimental data.[7,58,59] The use of numerical simulations in studying the Turing pattern formation seems promising since computationally one may study system that are beyond the reach of experiments and the numerical data is more accurate and easier to analyze as compared to experimental data.[60,61]

This article reviewed some rather theoretical methods that are generally used in analyzing the dynamical behavior of reaction-diffusion systems. The linear analysis is efficient in predicting the presence of instability and the characteristic length of the resulting patterns. However, linear analysis does not reveal anything about the morphology of the resulting pattern. To study the pattern or structure selection we employed the nonlinear bifurcation analysis, which approximately predicts the stability of different symmetries, i.e., the parameter regime that results in certain

Turing structures. If one uses homogeneous random initial conditions there is no way to predict the selection of the phase of the resulting pattern (the positions and alignment of stripes or spots). A further difficulty arises if one has to study the pattern selection of a morphologically bistable system: if both stripes and spots are stable, there is no general way to determine, which of the states the system will choose. These inadequacies of the theory of pattern formation are in connection to the fundamental problem of non-equilibrium thermodynamics and remain to be answered both in context of Turing systems and also in the more general framework of non-equilibrium physics.

Acknowledgments

This work has been supported by the Finnish Academy of Science and Letters and Jenny and Antti Wihuri foundation.

References

1. P. Ball, *The self-made tapestry: pattern formation in nature*, (Oxford Univ. Press, Oxford, 2001).
2. M. C. Cross and P. C. Hohenberg, *Rev. Mod. Phys.* **65**, 851 (1993).
3. S. R. De Groot and P. Mazur, *Non-equilibrium Thermodynamics*, (North Holland, Amsterdam, 1962).
4. G. Nicolis and I. Prigogine, *Self-Organisation in Non-Equilibrium Chemical Systems*, (Wiley, New York, 1977).
5. I. Prigogine, *Bull. Acad. Roy. Belg. Cl. Sci.* **31**, 600 (1945).
6. R. Landauer, *Phys. Rev. A* **12**, 636 (1975).
7. R. Kapral and K. Showalter (Eds.), *Chemical Waves and Patterns*, (Kluwer Academic Publishers, Dordrecht, 1995).
8. R. Kapral, *Physica D* **86**, 149 (1995).
9. N. Rashevsky, *Mathematical Biophysics*, (University of Chicago Press, Chicago, 1938).
10. A. M. Turing, *Phil. Trans. R. Soc. Lond.* **B237**, 37 (1952).
11. J. D. Murray, *Mathematical Biology*, (Springer-Verlag, Berlin, 1989).
12. J. D. Murray, *Mathematical Biology II: Spatial Models and Biomedical Applications*, (Springer-Verlag, Berlin, 2003).
13. A. J. Koch and H. Meinhardt, *Rev. Mod. Phys.* **66**, 1481 (1994).
14. I. Lengyel, Gyula Rabai and I. R. Epstein, *J. Am. Chem. Soc.* **112**, 4606 (1990); ibid. 9104.
15. J. A. Vastano, J. E. Pearson, W. Horsthemke and H. L. Swinney, *J. Chem. Phys.* **88**, 6175 (1988).
16. I. Lengyel and I. R. Epstein in Ref. 7, p. 297.
17. V. Castets, E. Dulos, J. Boissonade and P. De Kepper, *Phys. Rev. Lett.* **64**, 2953 (1990).
18. Q. Ouyang and H. L. Swinney, *Nature* **352**, 610 (1991).
19. T. Leppänen, M. Karttunen, K. Kaski and R. A. Barrio, *Int. J. Mod. Phys. B* **17**, (2003).
20. Y. Astrov, E. Ammelt, S. Teperick and H.-G. Purwins, *Phys. Lett. A* **211**, 184 (1996).
21. J. Falta, R. Imbihl and M. Henzler, *Phys. Rev. Lett.* **64**, 1409 (1990).

22. J. Temmyo, R. Notzel and T. Tamamura, *Appl. Phys. Lett.* **71**, 1086 (1997).
23. M. Tlidi, P. Mandel and M. Haelterman, *Phys. Rev. E* **56**, 6524 (1997).
24. D. Walgraef and N. M. Ghoniem, *Phys. Rev. B* **67**, 064103 (2003).
25. R. A. Barrio, J. L. Aragon, C. Varea, M. Torres, I. Jimenez and F. Montero de Espinosa, *Phys. Rev. E* **56**, 4222 (1997).
26. J. A. Vastano, J. E. Pearson, W. Horsthemke and H. L. Swinney, *Phys. Lett. A* **124**, 320 (1987).
27. P. Gray and S. K. Scott, *Chem. Eng. Sci.* **38**, 29 (1983).
28. P. Gray and S. K. Scott, *Chem. Eng. Sci.* **39**, 1087 (1984).
29. P. Gray and S. K. Scott, *J. Phys. Chem.* **89**, 22 (1985).
30. J. E. Pearson, *Science* **261**, 189 (1993).
31. A. Gierer and H. Meinhardt, *Kybernetik* **12**, 30 (1972).
32. A. Hunding, *J. Chem. Phys.* **72**, 5241 (1980).
33. W. Vance and J. Ross, *J. Phys. Chem. A* **103**, 1347 (1999).
34. V. Dufiet and J. Boissonade, *J. Chem. Phys.* **96**, 664 (1991).
35. V. Dufiet and J. Boissonade, *Physica A* **188**, 158 (1992).
36. P. Borckmans and A. De Wit and G. Dewel, *Physica A* **188**, 137 (1992).
37. I. Lengyel and I. R. Epstein, *Science* **251**, 650 (1991).
38. I. Lengyel and I. R. Epstein, *Proc. Nat. Acad. Sci.* **89**, 3977 (1992).
39. R. A. Barrio and C. Varea and J. L. Aragón and P. K. Maini, *Bull. Math. Biol.* **61**, 483 (1999).
40. G. Nicolis, *Introduction to nonlinear science*, (Cambridge University Press, Cambridge, 1995).
41. S. Strogatz, *Nonlinear Dynamics and Chaos*, (Perseus, USA, 1994).
42. T. Leppänen and M. Karttunen and K. Kaski and R. A. Barrio and L. Zhang, *Physica D* **168-169**, 35 (2002).
43. J. Boissonade, E. Dulos and P. De Kepper in Ref. 7, p. 221.
44. A. C. Newell, T. Passot and J. Lega, *Annu. Rev. Fluid Mech.* **25**, 399 (1993).
45. J. D. Crawford, *Rev. Mod. Phys.* **63**, 991 (1991).
46. P. Manneville, *Dissipative Structures and Weak Turbulence*, (Academic Press, USA, 1990).
47. D. Walgraef, *Spatio-temporal Pattern Formation*, (Springer-Verlag, USA, 1997).
48. A. Rovinsky and M. Menzinger, *Phys. Rev. A* **46**, 6315 (1992).
49. N. W. Ashcroft and N. D. Mermin, *Solid State Physics*, (Harcourt Brace College Publishers, USA, 1976).
50. T. K. Callahan and E. Knobloch, *Phys. Rev. E* **53**, 3559 (1996).
51. T. K. Callahan and E. Knobloch, *Nonlinearity* **10**, 1179 (1997).
52. T. K. Callahan and E. Knobloch, *Physica D 132*, 339 (1999).
53. B. Dionne, M. Silber and A. C. Skeldon, *Nonlinearity* **10**, 321 (1997).
54. E. Kreyszig, *Advanced Engineering Mathematics*, 7th Ed. (Wiley, USA, 1993).
55. P. Borckmans, G. Dewel, A. De Wit and D. Walgraef in Ref. 7, p. 323.
56. S. Kondo and R. Asai, *Nature* **376**, 678 (1995).
57. A. L. Kawczynski and B. Legawiec, *Phys. Rev. E* **64**, 056202 (2001).
58. P. Borckmans, G. Dewelm, A. De Wit, E. Dulos, J. Boissonade, F. Gauffre and P De Kepper, *Int. J. Bif. Chaos* **12**, 2307 (2002).
59. I. Berenstein, L. Yang, M. Dolnik, A. M. Zhabotinsky and I. R. Epstein, *Phys. Rev. Lett.* **91**, 058302 (2003).
60. A. De Wit, P. Borckmans and G. Dewel, *Proc. Nat. Acad. Sci.* **94**, 12765 (1997).
61. T. Leppänen, M. Karttunen, K. Kaski and R. A. Barrio, *Prog. Theor. Phys. (Suppl.)* **150**, 367 (2003).